APPENDIX A

Synthetic Datasets

Synthetic datasets were computed for this thesis using the analytical ray tracing formulas. Models consisted of dipping linear reflectors in constant velocity and linear depth velocity media. Traveltime equations for separated source and receivers were adapted from Slotnick (1959). A three point wavelet (1,3,1) was convolved onto the traveltimes.

Constant Velocity Media

Equation (A.1) is the traveltime of a dipping linear reflector for the geometry of Figure A.1.

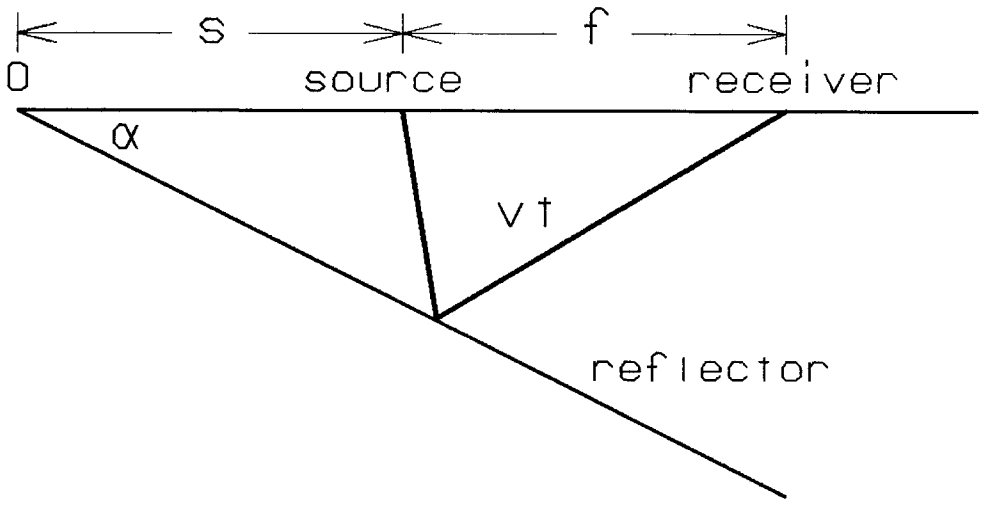

FIGURE A.1: Ray tracing in constant velocity media. Geometry for ray tracing in constant velocity media. The distance between the source and where the reflector intersects the surface is s. The source - receiver offset is f.

$$t = \frac{1}{v}\sqrt{f^2 + 4s\sin^2\alpha(s+f)} \qquad \text{(A.1)}$$

It is derived by putting a mirror image of the seismic experiment on the other side of the reflector.

Linear Depth Velocity Media

Given a linear increasing depth velocity function of the form $v_0 + az$, Slotnick showed that the raypath to a dipping reflector is a circular arc with a travel time

$$t = \frac{1}{a}\cosh^{-1}\left[1 + \frac{a^2(x^2 + z^2)}{2v_0(v_0 + az)}\right] \qquad \text{(A.2)}$$

The total travel time is the sum of that along raypaths from the source and receiver meeting at the reflector as shown in Figure A.2.

$$t = \frac{1}{a}\left\{\cosh^{-1}\left[1 + \frac{a^2[(s + f - x)^2 + (x\tan\alpha)^2]}{2v_0(v_0 + ax\tan\alpha)}\right]\right\} + \qquad \text{(A.3)}$$

$$\left\{\cosh^{-1}\left[1 + \frac{a^2[(x - s)^2 + (x\tan\alpha)^2]}{2v_0(v_0 + ax\tan\alpha)}\right]\right\}$$

Since x is unknown in equation (A.3), it is constrained by Fermat's principle to give

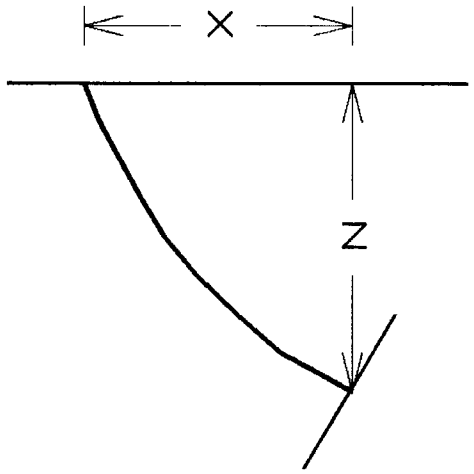

FIGURE A.2: Zero offset linear velocity media. Ray tracing for zero offset experiment in linear increasing depth velocity media.

the minimum travel time. This equation is difficult to solve analytically, so a searching method was used during the computation of the seismograms.

Some other useful formulas for linear increasing depth velocity media are zero offset two way travel time as a function of depth,

$$t(z) = \frac{2}{a}\ln\left[\frac{v_0 + az}{v_0}\right] \tag{A.4}$$

depth as a function of zero offset two way travel time,

$$z = \frac{v_0}{a}(e^{\frac{at}{2}} - 1) \tag{A.5}$$

interval velocity as a function of non-zero offset two way travel time,

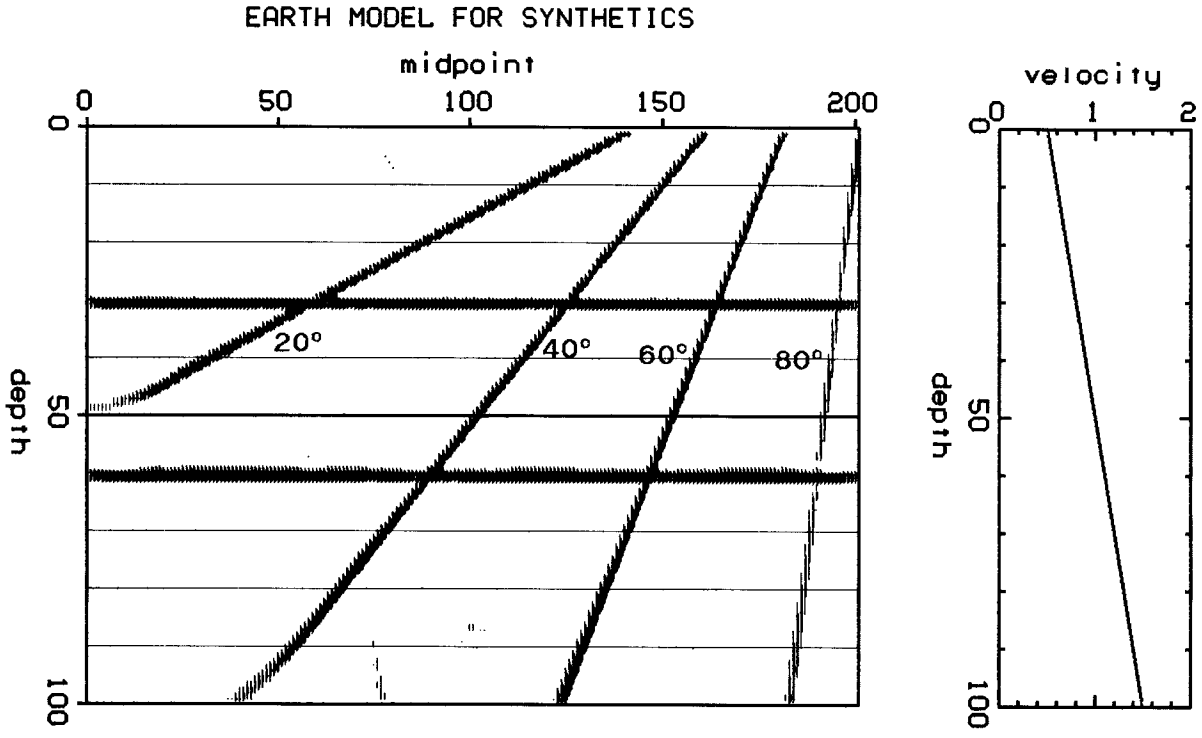

FIGURE A.3: Earth model for synthetics. This model consists of two flat reflectors and four dipping reflectors up to 80 degrees. The velocity increases linearly with depth.

$$v(t,f) = v_0 \left[\cosh \frac{at}{2} + \sqrt{\cosh^2 \frac{at}{2} - \frac{a^2 f^2}{4 v_0^2 2} - 1} \right] \qquad \text{(A.6)}$$

$$= v_0 e^{\frac{at}{2}} \quad \text{(for zero offset)}$$

and root mean squared velocity.

$$v_{rms}(t) = v_0 \left(\frac{e^{at} - 1}{at} \right)^{1/2} \qquad \text{(A.7)}$$

Common midpoint gathers were computed at every midpoint in the model shown in Figure A.4. Parameters are: #midpoints = 200; spacing = .5; #offsets = 100; spacing = 1.6; #time samples = 256; sample rate = 1.; v_0 = .5; a = .01. Selected common midpoint gathers and common offset midpoint sections are shown in Figures A.4 and A.5.

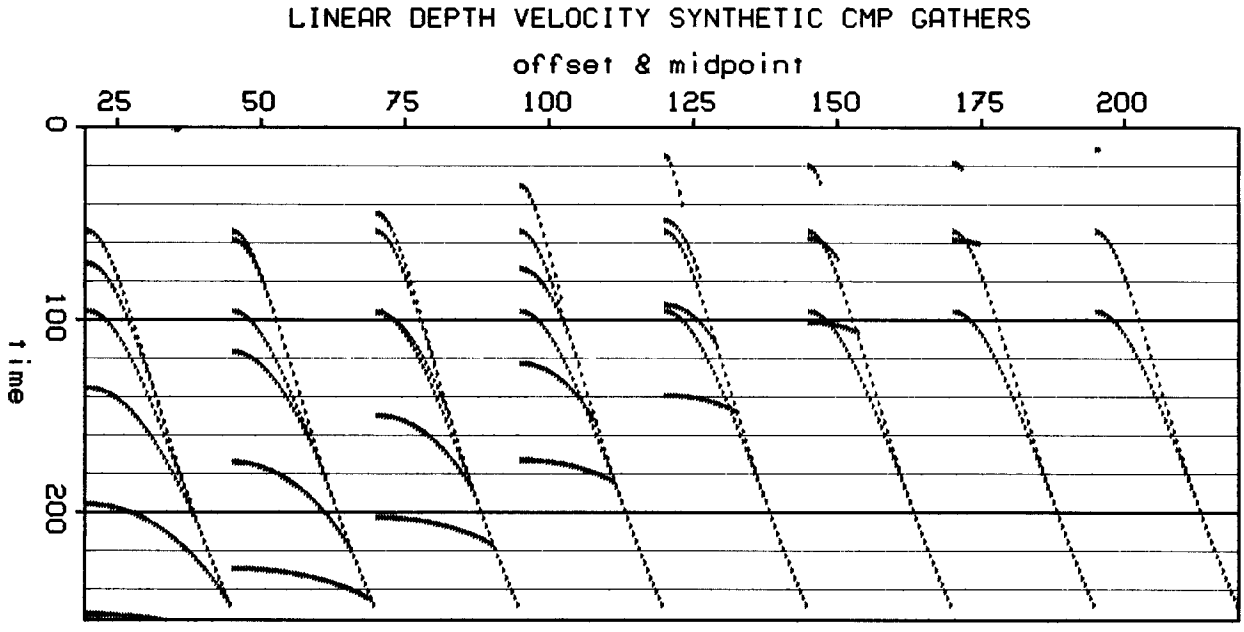

FIGURE A.4: Synthetic common midpoint gathers. Selected common midpoint gathers generated by equation (A.3) for model in Figure A.3.

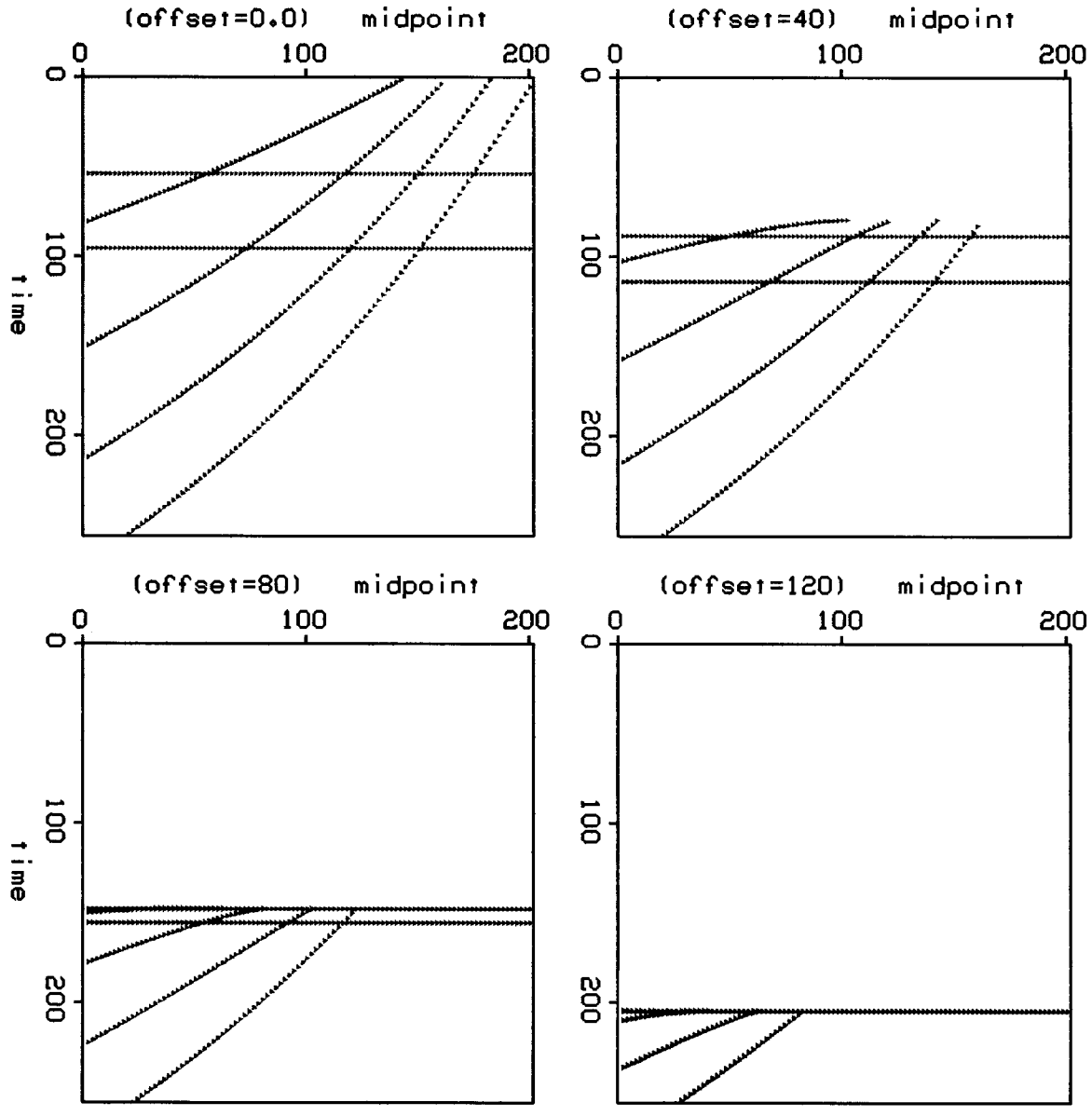

FIGURE A.5: Synthetic constant offset sections. Selected constant offset sections generated by equation (A.3) for model in Figure A.3.

APPENDIX B

How to Construct Good Midpoint Slant Stacks

The chief practical problem of midpoint slant stack migration is obtaining slant stacks free of obscuring artifacts. The two main causes of artifacts are offset aliasing and truncation of data at the ends of offset spreads. Offset aliasing means that offsets are too coarsely sampled for some wave propagation angles to be cleanly imaged on slant stacks. Figure B.1 shows that these artifacts are manifested as diagonal lines across slant stack gathers. On midpoint slant stack sections, these artifacts appear as false horizontal events. In addition, Figure B.1 shows that offset truncation can falsify the time of a reflection in a slant stack. Truncations can also add diagonal linear artifacts to slant stack gathers.

Schultz (1978) recommended applying mutes and tapers to the dataset in order to avoid truncation and aliasing artifacts. The technique determining mutes is similar to computing Snell trace trajectories described in chapter 4. The problem with this approach is that it assumed some velocity model for the dataset. Then the velocity independent advantage of slant stacking is undercut. Having to chose a particular velocity model fails for the same reasons as for CMP stacking. Dipping reflectors have an apparent high velocity, leading to velocity ambiguity. Also when reflectors of two different dips coincide on a CMP gather, the velocity model becomes unworkably multi-valued.

Our approach is to extrapolate seismic traces between existing traces to counter aliasing and beyond existing offsets to counter truncation. We use velocity insensitive extrapolation techniques where possible in order to avoid introducing a velocity bias into the data.

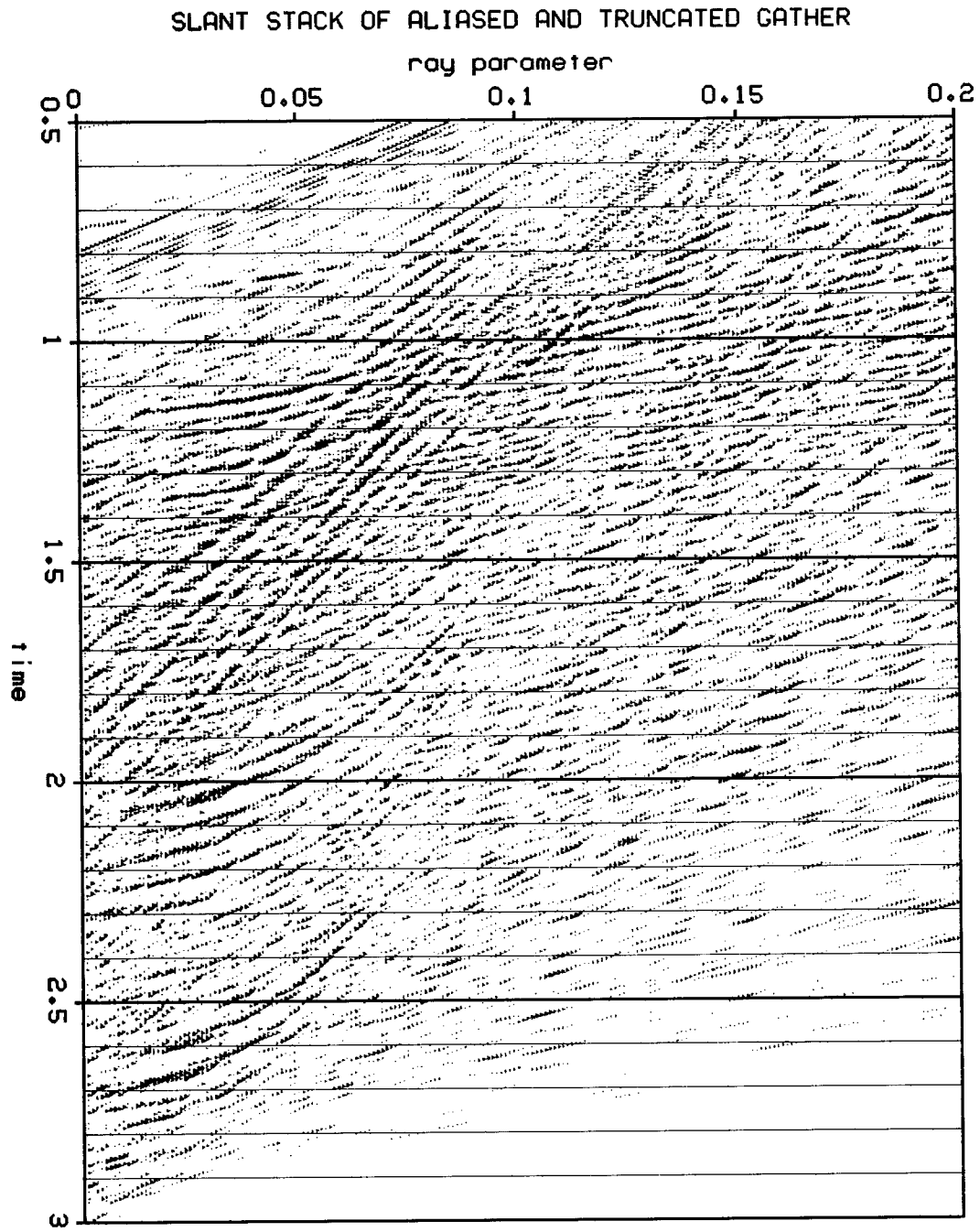

FIGURE B.1: Slant stack of aliased and truncated CMP gather. The linear artifacts are caused by the CMP gather offsets being too far apart. Missing near offsets falsifies the times of real reflection events. The elliptical shaped events should intersect the left axis perpendicularly, but do not. Missing near offsets also lead to missing reflections in the upper left hand corner. Missing wide offsets also falsify event times and have missing reflections, shown in the lower right part of the gather.

(1) To extrapolate in between offsets, we use the tilted interpolator method of Hale (1979). A one dimensional cubic spline is applied along a line tilted at the expected dip of the data. The dip prediction need not be very accurate and is therefore only weakly velocity dependent.

(2) Burg's method (1976) is used to extrapolate offsets beyond the end of a cable. Burg's method is nice because is predicts amplitude trends. This method works best when the dataset is statistically stationary. To make the data appear more stationary, we straighten curved reflections, apply a Fourier transform over time, and raise each sample to a fractional power. Normal moveout* is used to straighten inner offsets, while a squared-offset, squared-time resampling is used for the wider offsets.

(3) To further help truncation problems, an offset dependent taper is applied to 5 or 10 edge offsets.

Figure B.2 shows the slant stacks of the same CMP gather as used for Figure B.1, this time extrapolated. The improvement is astounding.

* Normal moveout applies a time shift which makes a non-zero offset trace look like a zero-offset trace.

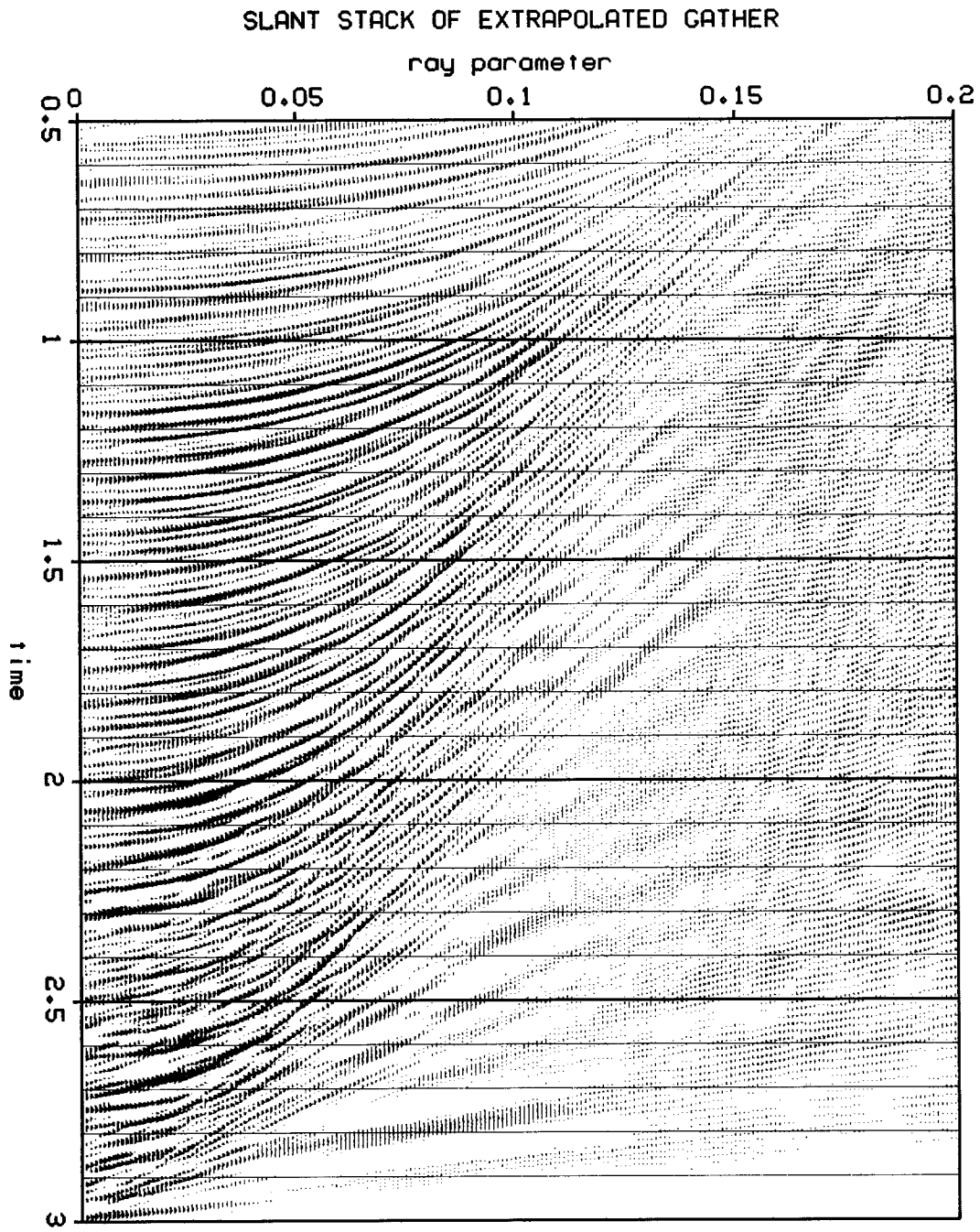

FIGURE B.2: Slant stack of extrapolated CMP gather. The CMP gather used in the previous figure was extrapolated from 24 to 106 offsets. Three offsets were interpolated between each existing offset and eight missing inner offsets were extrapolated. Also the five innermost and outermost offsets and direct arrival were tapered. Most of the slant stack artifacts in the previous figure have been reduced, leaving cleaner and more accurate slant stacks.

APPENDIX C

Frequency Domain Slant Stacking

Equation (2.6) leads to an inexpensive way of constructing slant stack gathers in the frequency domain.

$$\frac{k_h}{\omega} = -2\,p \tag{2.6}$$

This equation is a straight line in two dimensional Fourier coordinates (k_h,ω). The procedure for slant stacking in the frequency domain is

(1) Fourier transform the CMP gather in two dimensions, $h \rightarrow k_h$ and $t \rightarrow \omega$.

(2) Extract slant stacks for as many ray parameters p as desired by interpolating along the trajectories of equation (2.6), $k_h \rightarrow p$.

(3) While in the frequency domain, apply a coordinate transformation correction which is the Jacobian $|\omega|$ (Thorson, 1978).

(4) Finally, Fourier transform back into the time domain, $\omega \rightarrow t$.

APPENDIX D

On Selecting the Ray Parameter Values

Reasons for More Than One Ray Parameter

Theoretically, the structural image (traveltimes) of the earth's subsurface should be the same on each migrated angle-midpoint section independent of ray parameter. However, there are several reasons for migrating sections for more than one ray parameter. These reasons hold true for both slant stacks and Snell traces.

(1) One can perform velocity analysis, either before or after migration, using different ray parameter sections. The traveltimes to a given reflection will vary between different ray parameters if the dataset is unmigrated or migrated for an incorrect velocity model. Equations giving these variations as a function of velocity are given in chapters 2 and 4.

(2) One major cause of differences between angle-midpoint sections are missing near and wide offsets in the typical reflection seismic survey. This results in missing data on certain parts of angle-midpoint sections. Figure B.1 illustrates this problem. Summing several different ray parameter sections together will fill the blank spots.

(3) Summing several migrated angle-midpoint sections together increases signal to noise.

(4) Summing different ray parameter sections together increases lateral resolution. Bolondi et. al. (1981) demonstrated that each offset ($\approx$ ray parameter) has a different spatial frequency content. Summing together more than one *correctly migrated* offset section enhances the overall lateral resolution.

(5) In some processing schemes one might want to invert angle-midpoint sections back into constant offset sections (chapter 3). A range of different ray parameters is necessary to recover a range of offsets.

(6) Outside the scope of this thesis, yet important, are the amplitude variations between different angle-midpoint sections. This amplitude information contains stratigraphic information.

Ray Parameter Range

The ray parameter range should fit that of the data. In the case of slant stacks the ray parameters are the time slopes of events on a common midpoint gather. There is a minimum and maximum time slope depending upon the offsets in the common midpoint gather and the subsurface velocity structure (Figure D.1). In no case should the largest ray parameter be greater the inverse of the lowest velocity in the data.

In the case of Snell traces, the ray parameter is related to the trajectory of the radial trace. The small ray parameter Snell traces will go through the short (perhaps non-existent) offsets. Likewise, large ray parameter Snell traces may be mostly off the cable.

In this thesis the minimum and maximum ray parameters were such that no more than 50 percent of the slant stack or Snell trace were blank.

Number of Ray Parameters

Summing together more than one angle-midpoint section increases signal to noise. However, each additional angle-midpoint section means the cost of an extra migration.

The signal to noise increase of a slant stack lies between that of a single unstacked trace and a common midpoint stack. Slant stacking sums together data across the width of a Fresnel zone (Figure 2.6) which is usually several traces wide

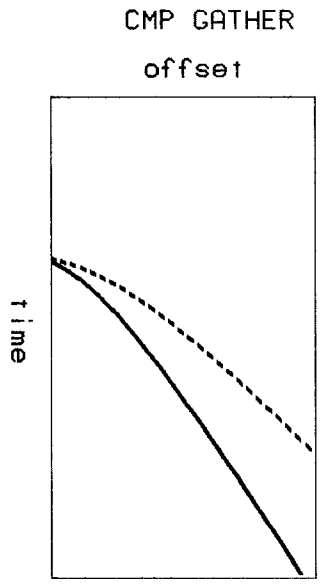

FIGURE D.1: Ray parameter bandwidth of CMP gather. If a reflection has a given time slope, then it will appear on a slant stack for the ray parameter equal to that slope. Missing inner offsets, which have shallow slopes, put a minimum bound on the ray parameter range. The widest offset or the slope of the wide angle hyperbola asymptote suggests a maximum ray parameter. Steep dipping events (dashed line) will slant stack at the lower ray parameters.

on a common midpoint gather. This means that the number of ray parameters can be less than the number of offsets in a common midpoint gather.

However, Snell traces do not have any signal increase over unstacked traces. In this case, as many ray parameters as offsets should be used for noise reduction. To reduce the number of migrations, one could substack several adjacent Snell traces. To improve the quality of the substacks, one could apply a moveout correction to each Snell trace. Fortunately, the moveout correction is a time independent constant. That is because the ray parameter of the substack (the ray parameter of the middle Snell trace) is the time slope of the data and determines the moveout correction.

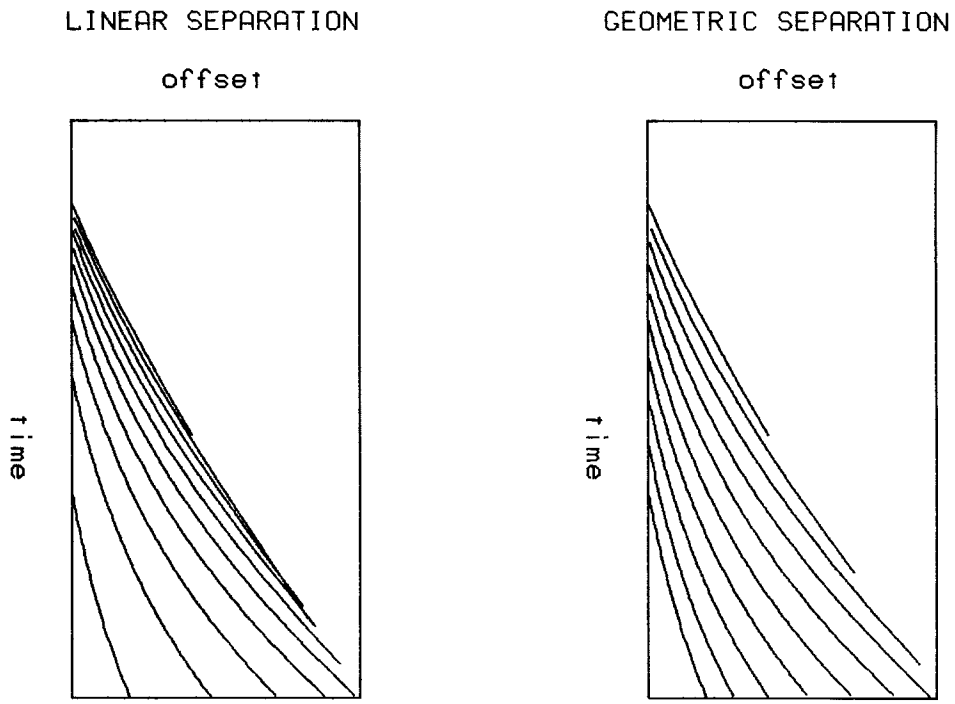

FIGURE D.2: Snell trace separation. These are Snell trace trajectories across a CMP gather with linearly increasing depth velocity. On the left the interval between ray parameters is the same. Here there is a bunching of trajectories at wide offsets. On the right the interval between Snell traces increases geometrically by a factor 1.2. It is more evenly sampled.

Distribution of Ray Parameters

Choosing ray parameters at fixed intervals causes the Snell traces to bunch up at wide offsets (Figure D.2). If the dataset is sampled too much in one area, then the signal to noise may not be improved too much after stacking. The magnitude of this problem depends on how rapidly velocity varies with depth. A geometrically increasing interval between ray parameters improves the sampling (Figure D.2). This means that the sampling is biased toward smaller ray parameters.

Bolondi et. al. (1981) found when it comes to enhancing lateral resolution, an even offset-squared distribution is better than an even offset distribution. That means to more closely sample wide offsets than near offsets. Since offset is

directly proportional to ray parameter (equation (4.4)), an even ray parameter-squared distribution may best enhance lateral resolution. Note that this suggestion conflicts with that of the previous paragraph.

APPENDIX E

The Double Square Root Equation

The *double square root equation* is used to extrapolate into the earth the wavefield recorded by separated sources and receivers located at the earth's surface.

Derivation

The derivation begins with the differential equation which extrapolates a time varying wavefield P in the depth z direction

$$\frac{\partial P}{\partial z} = \left[\frac{\partial t}{\partial z} \right] \frac{\partial P}{\partial t} \tag{E.1}$$

The bracketed expression is the change of wavefield traveltime with depth. It incorporates the geometry of the sources and receivers. Depth variable velocities can be handled by successively propagating across thin constant velocity layers.

Consider the case of a slanted plane wave recorded by an array of receivers as shown in Figure E.1. The lateral coordinate is denoted by g, standing for geophone coordinate. Figure E.1 shows that the change in wavefield traveltime with depth is

$$\frac{\partial t}{\partial z} = \frac{\cos\theta}{v} \tag{E.2}$$

The statement of Snell's law in the frequency domain

$$\frac{\sin\theta}{v} = p = \frac{k_g}{\omega} \tag{E.3}$$

is used to rewrite $\cos\theta$ in quantities k_g and ω which are measurable from the recorded wavefield. Inserting equations (E.2) and (E.3) into equation (E.1) and Fourier transforming over time gives the depth extrapolation equation for plane waves.

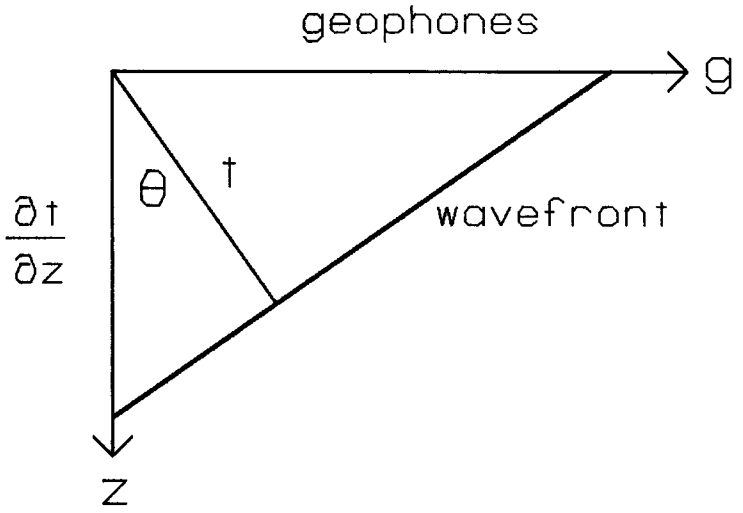

FIGURE E.1: Slant plane wave. Geometry of a slanted plane wave recorded by a row of geophones.

$$\frac{\partial P}{\partial z} = i\frac{\omega}{v}\left[1 - \left(\frac{vk_g}{\omega}\right)^2\right]^{1/2} P \qquad \text{(E.4)}$$

Equation (E.4) generalizes to wavefields more complex than plane waves by computing it for every value of k_g and ω.

The next step is to determine $\partial t / \partial z$ for an array of both sources and receivers. The lateral coordinate of the sources is named s, also known as the shot coordinate. The wavefield traveltime is expanded to include both sources and receivers.

$$dt = \frac{\partial t}{\partial z_g} dz_g + \frac{\partial t}{\partial z_s} dz_s \qquad \text{(E.5)}$$

All three depth coordinates are the same.

$$z_g = z_s = z \qquad \text{(E.6)}$$

$\partial t \; / \; \partial z_g$ is the same as for equation (E.4).

$$\frac{\partial t}{\partial z_g} = \left[\left(\frac{1}{v}\right)^2 - \left(\frac{k_g}{\omega}\right)^2\right]^{1/2} \qquad \text{(E.7)}$$

The reciprocity principle is invoked to find the other term.

$$\frac{\partial t}{\partial z_s} = \left[\left(\frac{1}{v} \right)^2 - \left(\frac{k_s}{\omega} \right)^2 \right]^{1/2} \tag{E.8}$$

Inserting equations (E.5) through (E.8) into equation (E.1) gives the double square root equation for depth extrapolation of a wavefield recorded by separated sources and receivers.

$$\frac{\partial P}{\partial z} = -i \frac{\omega}{v} \left[\sqrt{1 - G^2} + \sqrt{1 - S^2} \right] P \tag{E.9}$$

G and S are shorthand for the wavenumber ratios

$$G = \frac{v k_g}{\omega} \qquad S = \frac{v k_s}{\omega} \tag{E.10}$$

The extra minus sign in equation (E.9) provides the correct direction of extrapolation for a reflection seismology geometry.

Midpoint-Offset Coordinates

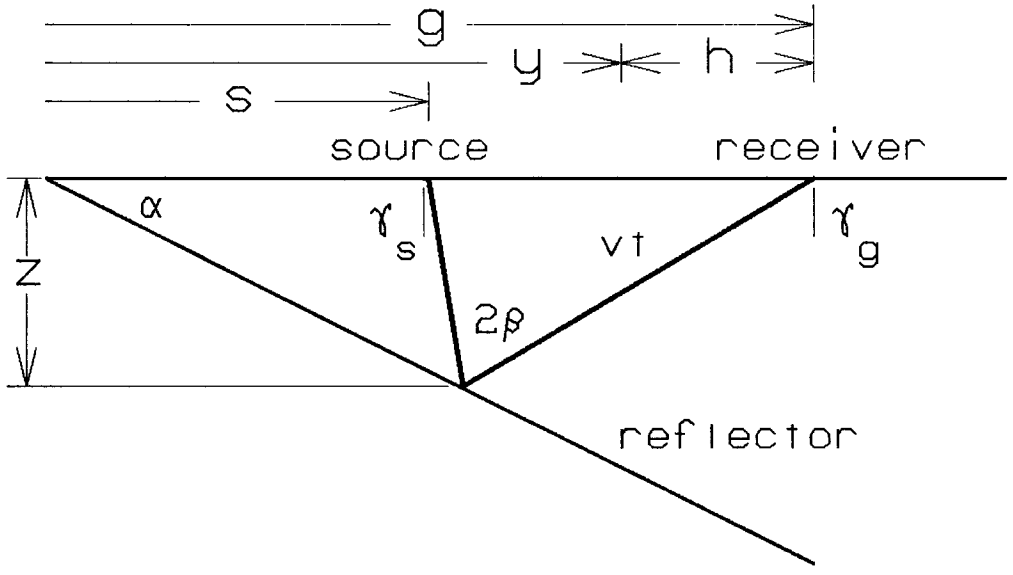

FIGURE E.2: Geometry of reflection seismology experiment. Lateral coordinates are s for the shot coordinate, g for the geophone coordinate, y for the source-receiver midpoint, and h for the half offset. Earth angles include dip α, reflector incidence raypath half angle 2β, and surface raypath incident angles γs and γg.

This thesis uses midpoint-offset coordinates (y,h) rather than field coordinates (s,g). The relation of these two coordinate systems is depicted in Figure E.2.

$$y = \frac{g + s}{2} \qquad h = \frac{g - s}{2} \tag{E.11}$$

To find the the equivalent wavenumber relations, we first perform a chain rule derivative expansion of field coordinates in terms of midpoint coordinates.

$$\frac{\partial P}{\partial g} = \frac{\partial P}{\partial y}\frac{\partial y}{\partial g} + \frac{\partial P}{\partial h}\frac{\partial h}{\partial y} = \frac{1}{2}\left[\frac{\partial P}{\partial y} + \frac{\partial P}{\partial h}\right] \tag{E.12}$$

$$\frac{\partial P}{\partial s} = \frac{\partial P}{\partial y}\frac{\partial y}{\partial s} + \frac{\partial P}{\partial h}\frac{\partial h}{\partial y} = \frac{1}{2}\left[\frac{\partial P}{\partial y} - \frac{\partial P}{\partial h}\right] \tag{E.13}$$

Then we Fourier transform equations (E.12) and (E.13) using the Fourier domain derivative rule and divide out an iP factor to obtain the desired relations.

$$k_g = \frac{k_y + k_h}{2} \qquad k_s = \frac{k_y - k_h}{2} \tag{E.14}$$

Inserting equations (E.19) into equation (E.9) gives the double square root equation in midpoint-offset coordinates.

$$\boxed{\frac{\partial P}{\partial z} = -i\frac{\omega}{v}\left[\sqrt{1-(Y-H)^2} + \sqrt{1-(Y+H)^2}\right]P} \tag{E.15}$$

As before, a shorthand is used.

$$H = \frac{vk_h}{2\omega} \tag{E.16}$$

Geometric Interpretation

The wavenumber ratios G, S, Y, and H have physical interpretations both in the earth and on the data. G and S are sines of angles according to Snell's law (equation (E.3)). These angles are the raypaths incident to the source and receiver as shown in Figure E.2.

$$G = \sin\gamma_g \qquad S = -\sin\gamma_s \tag{E.17}$$

The minus sign gives both angles the same direction of rotation.

Since midpoint and offset are not physical data recording dimensions, it is not readily apparent how to physically interpret Y and H in terms of earth angles. Figure E.2 gives the relation between reflector dip angle α, offset incident angle β, and wavefront angles γ_g and γ_s (derived by Rob Clayton).

$$\gamma_g = \beta + \alpha \qquad \gamma_s = \beta - \alpha \tag{E.18}$$

H and Y may be solved for in terms of α and β using equations (E.10), (E.14), (E.16), and (E.17).

$$Y = \sin\alpha \cos\beta \qquad H = \sin\beta \cos\alpha \tag{E.19}$$

Y is mostly reflector dip at small offsets. H is mostly offset angle when dips are small.

On seismic data, G, S, Y, and H are slopes of reflection events. G is the data slope on a shot profile (all of the records for a given shot). S is the data slope on a common geophone gather (all of the trace recorded at the same geophone location). Y is the slope on a midpoint section and H is the slope on a CMP gather.

Conventional Processing

The double square root equation (E.15) decomposes into operations describing conventional CMP stacking and migration of these stacks. A stacked section simulates zero offset. The offset angle β is zero. Then according to equation (E.19), H becomes zero. The double square root equation reduces to

$$\frac{\partial P}{\partial z} = -2i\frac{\omega}{v}\sqrt{1 - Y^2}\,P \tag{E.20}$$

Likewise, we obtain an equation for the conventional stacking of flat events by setting the reflector dip α equal to zero in equation (E.19). Y goes to zero and the double square root equation becomes

$$\frac{\partial P}{\partial z} = -2i\frac{\omega}{v}\sqrt{1 - H^2}\, P \qquad \text{(E.21)}$$

We have not been able to obtain a mathematically exact formula for stacking dipping reflectors. Permitting the $\cos\alpha$ part of H in equation (E.19) be non-zero is a first order correction identical to the cosine velocity correction. However, the assumption $Y = 0$ used in deriving equation (E.21) is then wrong. Various alternatives to CMP stack migration which implement the double square equation more effectively are discussed in this thesis.

APPENDIX F

Stationary Phase Derivation of Radial Trace Migration Equation

The purpose of this derivation threefold:

(1) It is a direct way of deriving the radial trace migration operator from the wave equation. However, this derivation is not as clear or simple as the one given in chapter 3.

(2) It gives amplitude corrections which should be applied during migration.

(3) It shows how the constant offset migration methods of Hale (1983) relate to the methods of this thesis.

Much of this derivation directly follow's Hale's thesis (1983).

Migration Integral

We begin with Stolt's (1978) migration algorithm.

$$P(k_z,k_y,k_h) = \left[\frac{\partial \omega}{\partial k_z}\right] P(\ \omega(k_z,k_y,k_h)\ ,k_y,k_h) \qquad \text{(F.1)}$$

Migration is essentially a frequency domain shift from the time axis to the depth axis. The shift is given by the dispersion relation $\omega(k_z,k_y,k_h)$. Hale suggests doing the frequency domain shift in the following integral to avoid wavenumber interpolation.

$$P(k_z,k_y,k_h) = \int dt\ P(t,k_y,k_h) \left[\frac{\partial \omega}{\partial k_z}\right] e^{it\,\omega(k_z,k_y,k_h)} \qquad \text{(F.2)}$$

This is the basic migration integral. In order to migrate radial traces, which are the data at a constant ratio of offset to time, we need to inverse Fourier this integral to offset.

$$P(k_z,k_y,h) = \int dt\ P(t,k_y,h) \int dk_h \left(\frac{\partial \omega}{\partial k_z}\right) e^{it\,\omega(k_z,k_y,k_h) - ik_h h} \qquad \text{(F.3)}$$

When we solve the k_h integral we will again obtain a migration equation of the form of equation (F.2) except with a new dispersion relation $w(k_z,k_y,h)$.

Stationary Phase Solution of Migration Integral

The greatest contribution to the k_h integral in equation (F.3) is when the exponential phase is most slowly changing, i.e. at minimum phase. The phase, denoted by Θ, is

$$\Theta = \omega t - k_h h \qquad \text{(F.4)}$$

where the dispersion relation $w(k_z,k_y,k_h)$ comes from the double square root equation (F.21).

$$\omega = \frac{v}{2}\left[\, k_y^2 + k_z^2 + k_h^2 \left(1 + \frac{k_y^2}{k_z^2}\right) \right]^{1/2} \qquad \text{(F.5)}$$

The stationary point is at

$$\frac{\partial \Theta}{\partial k_h} = 0 \qquad \text{(F.6)}$$

$$\frac{\partial \omega}{\partial k_h} = \frac{h}{t}$$

A fair amount of algebra leads to the solutions

$$\hat{k}_h = \frac{2h}{vt} k_z^2 \left[\, k_y^2 + k_z^2 \left(1 - \frac{4h^2}{v^2 t^2}\right) \right]^{-1/2} \qquad \text{(F.7a)}$$

$$\hat{\omega} = \frac{v}{2}\left[\, k_y^2 + k_z^2 \right] \left[\, k_y^2 + k_z^2 \left(1 - \frac{4h^2}{v^2 t^2}\right) \right]^{-1/2} \qquad \text{(F.7b)}$$

$$\hat{\Theta} = \frac{vt}{2}\left[\, k_y^2 + k_z^2 \left(1 - \frac{4h^2}{v^2 t^2}\right) \right]^{1/2} \qquad \text{(F.7c)}$$

where the hat denotes the quantities evaluated at the stationary point.

The general stationary phase solution is given by (from Carrier, et. al.)

$$\int_{-\infty}^{+\infty} dx\ \Phi(x)\, e^{i\Theta(x)} \approx \left[\frac{2\pi}{|\Theta(\hat{x})''|}\right]^{1/2} \Phi(\hat{x})\, e^{i\Theta(\hat{x}) \pm \frac{i\pi}{4}}$$

Specifically, equation (1.3) becomes

$$P(k_z,k_y,h) = \int dt\ P(t,k_y,h)\ \alpha\ \omega^{-1}\ e^{it\omega + \frac{i\pi}{4}} \tag{F.8}$$

where

$$\omega = \frac{v}{2}\left[\ k_y^2 + k_z^2\ (1 - \frac{4h^2}{v^2t^2})\ \right]^{1/2} \tag{F.9}$$

$$\alpha = \frac{vt}{\omega}\left[\frac{2\pi\ (k_y^2 + k_z^2)}{\omega}\right]^{1/2}$$

Equation (F.9) is the dispersion relation for migrating constant offset sections. Hale uses a modification of this equation for the purposes of his thesis.

Radial Trace Migration Equation

The dispersion relation in the radial trace migration equation is the same as equation (F.9). The radial trace migration equation from chapter 3 is

$$\frac{\partial P}{\partial z} = -i\left[\frac{\frac{4\omega^2}{v^2} - k_y^2}{1 - \frac{4r^2}{v^2}}\right]^{1/2} P \tag{3.5}$$

The dispersion relation of this equation is

$$k_z^2 = \frac{\frac{4\omega^2}{v^2} - k_y^2}{1 - \frac{4r^2}{v^2}} \tag{F.10}$$

It is simple algebra to verify that equations (F.9) and (F.10) are the same if the radial trace definition $r = h/t$ is made.

Therefore, equation (F.8) may be used to migrate radial trace sections. Unlike equation (3.5), this new migration equation describes an amplitude correction due to translation into radial trace coordinates.

APPENDIX G

Migration Implementation

The phase shift method (Gazdaz, 1979) was used to implement the migration equations presented in this thesis. It is the most accurate method for dips to 90 degrees in depth variable velocity media, although it is relatively slow.

The migration equations presented in this thesis were first order differential equations of the form

$$\frac{\partial P(\omega,z,\underline{k})}{\partial z} = -i\frac{\omega}{v}\Phi(\omega,z,\underline{k})\,P(\omega,z,\underline{k}) \qquad \text{(G.1)}$$

To avoid numerical complications when choosing the dz size, equation (G.1) is transformed to zero offset coordinates $d\tau = v(z)dz$.

$$\frac{\partial P}{d\tau} = -i\omega\,\Phi(\omega,\tau,\underline{k})\,P \qquad \text{(G.2)}$$

The solution to this equation is

$$P(\omega,\tau+\Delta\tau,\underline{k}) = P(\omega,\tau,\underline{k})\,e^{-i\omega\Phi\Delta\tau} \qquad \text{(G.3)}$$

Depth variable velocity media are modelled as a pile of thin constant velocity layers. Equation (G.3) extrapolates across each layer. The cumulative extrapolation is

$$P(\omega,\tau,\underline{k}) = P(\omega,\tau=0,\underline{k})e^{-i\omega\int_0^\tau d\tau\frac{\partial\Phi}{\partial\tau}} \qquad \text{(G.4)}$$

The extrapolation stops when the sources and receivers are just above the reflector. Here there is zero offset and zero travel time to the reflector. This is known as the imaging condition. The left hand side of equation (G.4) is inverse Fourier transformed for zero travel time to obtain an image. Zero time in the frequency domain is just the sum of all frequencies.

$$P(\omega,\tau,\underline{k}) = \sum_{\omega} P(\omega,\tau=0,\underline{k}) e^{-i\omega \int_0^{\tau} d\tau \frac{\partial \Phi}{\partial \tau}} \qquad \text{(G.5)}$$

Equation (G.5) is what is programmed into the computer.

Equation 5 implies that each output point is an inner product of a length equal to the number of frequencies. Therefore, the computation grows as the square of the number of time samples. Various shortcuts reduce the expense:

(1) There is a conjugate symmetry in the real-to-complex Fourier transform. Only half the exponentials need be computed.

(2) Real seismic data is band limited, so not all the frequencies need be computed.

(3) When velocity changes slowly with depth, $\partial\Phi / \partial\tau$ need not be computed every τ step.

(4) Lookup tables can be used for square roots and trig functions.

APPENDIX H

Migration of Field Coordinate Slant Stacks

Several other workers have suggested slant stack migration schemes (Ryabinkin, et. al., 1962; Schultz and Claerbout, 1978; Taner, 1978; Phinney and Jurdy, 1979; Garotta, 1980; Treitel et. al., 1981). All these schemes are similar to mine in that the migration of unstacked data is a two step process. First, some kind of slant stacks are constructed. Second, the slant stacks are migrated. The major difference between all of the above cited schemes and mine is that the slant stacks are made on shot profiles or common geophone gathers, while I use CMP gathers. The tradeoffs between the two coordinate systems have been discussed in chapter 1. In brief, midpoint coordinates are more workable than field coordinates, but field coordinates are able to handle lateral velocity variations better.

There are some other differences between the various schemes. Most perform the slant stacks in the computer, though it has been electronically (by time delays) in the seismic records during recording (Ryabinkin et. al. 1962). The migration stage uses either the wave equation (Schultz and Claerbout, 1978; Taner, 1978) or ray tracing (Rybinnkin et. al. 1972; Phinney and Jurdy, 1978).

I shall describe how two of the migrations may be done. (I am not certain, because details have not been fully published in English). Both of these descriptions proceed from the double square root equation (appendix E), which is a general formula for migrating unstacked data.

SIMPLAN

Taner's SIMPLAN* process (1978) slant stacks shot profiles. A mathematical description this kind of slant stacking is similar to that derived in section 2.3.

$$\frac{k_g}{\omega} = p_g \tag{H.1}$$

Since Taner is stacking accross geophone offset g instead of midpoint offset h, the lateral wave number and ray parameter are subscripted by g to denote the difference.

To obtain an equation for migrating shot profile slant stacks, we will begin with the double square root equation in field coordinates.

$$\frac{\partial P}{\partial z} = -i\frac{\omega}{v}\left[\sqrt{1 - G^2} + \sqrt{1 - S^2}\right] P \tag{E.9}$$

The definition of shot profile slant stacking, equation (H.6), resembles the definition of G given in equation (E.10).

$$G = \frac{k_g}{\omega} \tag{E.10}$$

An equation for migrating shot profile slant stacks is derived with replacing G in the double square root equation by the formula for shot profile slant stacking.

$$\boxed{\frac{\partial P}{\partial z} = -i\frac{\omega}{v}\left[\sqrt{1 - p_g^2 v^2} + \sqrt{1 - S^2}\right] P} \tag{H.2}$$

Equation 6 can be broken down into two operations. First, the slant stacks are migrated with a single square root operator $\sqrt{1 - S^2}$. This is the same operator used for migrating CMP stack sections, so already existing programs can be used. Second, a time shift correction $\sqrt{1 - p_g^2 v^2}$ is applied.

---

* Simplan is an abbreviation for SIMulated PLANe wave.

Controlled Directional Receptivity

This is one of the most popular migration methods used in the Eastern Block. This method begins by slant stacking both sides of a split spread profile. One side gives an estimate of p_g. Using the principle of reciprocity, the other side gives an estimate of p_s. Both estimates are needed to solve the double square root equation.

Interestingly enough, in practice CDR uses the midpoint offset form of the double square root equation (E.15) rather than the field coordinate form. Estimates for Y and H are obtained from the sum and differences of p_g and p_s.

$$Y = \frac{v}{2\omega}(p_g - p_s) \qquad H = \frac{v}{2\omega}(p_g + p_s) \tag{H.3}$$

Values of p_g and p_s are picked from the slanted stacks and inserted into a ray tracing solution to the double square root equation.

REFERENCES

Bessonova, E.N., Fishman, V.M., Ryaboyi, V.Z., and Sitnikova, G.A., 1974, The tau method for inversion of traveltimes: Geophysics Journal, v. 36, p. 377-398

Burg, J.P., 1975, Maximum entropy spectral analysis: Ph.D. thesis, Stanford, CA, 123 pages.

Bolondi, G., Loinger, E., and Rocca, F., 1981, Offset continuation of seismic sections: preprint from the 43rd EAEG meeting, Venice

Carrier, G.F., Krook, M., and Pearson, C.E., 1966, Functions of a complex variable: McGraw Hill, New York

Clayton, R.W., and McMechan, G.A., 1981, Inversion of refraction data by wavefield continuation: Geophysics, v. 46, no. 6, p. 860-868

Claerbout, J.F., 1976, Fundamentals of geophysical data processing: McGraw, N.Y.

Deregowski, S.M., and Rocca, F., 1981, Geometrical optics and wave theory of constant offset sections in layered media: Geophysical Prospecting, v. 29, p.374

Garotta, R., 1980, Bi-radial imaging and complicated tectonics: paper presented at the 42nd EAEG meeting, Istanbul

Gazdag, J., 1978, Wave equation migration with the phase shift method: Geophysics, v. 43, p. 1342-1351

Hale, I.D., 1980, Spatial interpolation of steep dips: personal communication

Hale, I.D., 1983, Dip moveout by Fourier transform, Ph.D. thesis, Stanford CA

Judson, D.R., Schultz, P.S., and Sherwood, J.W.C., 1978, Equalizing the stacking velocities of dipping events via Devilish: paper presented at the 48th Annual SEG meeting, San Francisco

Levin, F.K., 1971, Apparent velocity from dipping interface reflections: Geophysics, v. 36, no. 3, p. 510-516

Lynn, W.S. and Claerbout, J.F., 1982, Velocity estimation in laterally varying media: Geophysics, v. 47, no. 6, p. 884-897

McMechan, G.A. and Ottolini, R., 1980, Direct Observation of a p-τ curve in a slant stacked wavefield: Seismological Society of America Bulletin, v. 70, p. 775-789

Phinney, R.A., and Jurdy, D.M., 1979, Seismic imaging of the deep crust: Geophysics, v. 44, no. 10, p. 1637-1666

Ryabinkin, L.A., et. al., 1962, Theory and practice of the CDR seismic method (Russian): Gostoptekhizdat, Moscow

Schultz, P.S., and Claerbout, J.F., 1978, Velocity estimation and downward continuation by wavefront synthesis: Geophysics, v. 43, p. 691-741

Slotnick, M.M., 1959, Lessons in seismic computing: edited by R.A. Geyer, SEG, Tulsa

Taner, M.T., 1975, Long period multiples and their suppression: paper presented at the 45th SEG meeting, Denver

Taner, M.T., 1978, Simulating plane wave sections- an update: paper presented at the 48th SEG meeting, San Francisco

Treitel, S., Gutowski, P.R., and Wagner, D.E., 1982, Plane wave decomposition of seismograms: Geophysics, v. 47, no. 10, p. 1375-1401

Yilmaz, O., and Claerbout, J.F., 1980, Prestack partial migration: Geophysics, v. 45, p. 1753-1779